Ceramics International 51 (2025) 3370–3382

Contents lists available at ScienceDirect

Ceramics International

journal homepage: www.elsevier.com/locate/ceramint

Plasma formation during flash sintering of boron carbide – Part II: Effect on sintering and optimisation of process variables

Christian Bechteler [a], Sudarshan Narayanan [a,b], Richard I. Todd [a,*]

[a] University of Oxford, Department of Materials, Parks Road, Oxford, OX1 3PH, UK
[b] Indian Institute of Technology Kanpur, Department of Sustainable Energy Engineering, Kanpur, 208016, Uttar Pradesh, India

ARTICLE INFO

Handling Editor: Dr P. Vincenzini

Keywords:
Flash sintering
Boron carbide
Plasma
Densification
Carbides

ABSTRACT

Field assisted sintering techniques, such as Flash Sintering (FS), allow rapid heating and densification of ceramics within seconds at significantly reduced environmental temperatures. FS of oxides has been extensively researched since 2010, whereas the potential densification of non-oxides such as carbides is rarely investigated. In the first part of this investigation the atmospheric breakdown and plasma formation under FS-conditions relevant to SiC and B_4C was researched. In the present work, the FS of B_4C was investigated with and without plasma formation for comparison, and the influence and optimum combination of the other main FS-parameters determined. The results showed that at a furnace temperature of 1500 °C, it is possible to densify B_4C by DC FS with or without an initial plasma formation. However, though plasma formation did not itself lead to densification of the material, the plasma-induced removal of the B_2O_3-layer on the surface of the powder led to a significant improvement in subsequent densification during FS. The effect of the Ar-plasma generated in removing the surface oxide from B_4C-particles was confirmed by SEM and XPS. Other process variables such as carbon additives, thermal insulation and hold time also significantly influenced the densification of B_4C by FS. With the optimised conditions, 96 % dense B_4C, with a grain size of 10 μm and a hardness of 31 GPa (HV1) was produced by pressureless FS in 5 min at a furnace temperature of 1500 °C.

1. Introduction

Flash sintering (FS) of ceramics, in which a powder compact is heated by passing an electric current through it, was first proposed in 1922 [1] and was independently rediscovered by Cologna et al., in 2010 [2]. Since then, numerous investigations of the phenomenon have been published and most of them research the behaviour of oxide ceramics. Less attention has been paid to FS of semiconducting materials such as carbide ceramics. Due to the high sintering temperatures (~2000 °C) necessary to densify carbides, the potential energy and time savings through the use of FS rather than conventional sintering are even greater than they are for oxides.

Although considerable success has been reported in flash spark plasma sintering (FSPS) of carbide ceramics to high density, where an applied pressure is used to promote densification [3–6], pressureless FS, the subject of this publication, is potentially more versatile and involves less capital outlay. With conventional sintering, however, it is generally more difficult to achieve high density without externally applied pressure and most carbides require sintering aids for high densities to be achieved, primarily because of their covalent nature. This is also the case for FS. In the first report of FS of non-oxides, for example, Zapata-Solvas et al. [7] were only able to achieve a relative density (RD) of 70 % in SiC without sintering aids but using liquid phase, oxide sintering aids [7] achieved 88 % RD with an environmental temperature of 1170 °C. Gibson et al. [8] FSed SiC using boron (B) and carbon (C) sintering aids, which give better hardness and creep resistance than oxide sintering aids, and achieved a maximum RD of 95 % in a conventional alumina tube furnace operating at 1500 °C.

Whilst FS of SiC is clearly successful, the pressureless flash sintering of B_4C to high density has not been achieved. Rosenberger et al. [9] investigated pressureless FS of disk-shaped B_4C samples by applying fields up to ≈ 280 V/cm with an electrical power dissipation of 100 W (0.15 W/mm^3) and environmental temperatures of up to 550 °C. They reported only locally densified regions within the samples due to current concentration. Furthermore, the optimum amount of sintering aid, which for B_4C is usually an excess of C [10–13], was not determined in Ref. [9]. The sintering aid content has been shown to be important in FS SiC [8,14,15]. Adjustment of such process parameters may improve the

* Corresponding author.
E-mail address: richard.todd@materials.ox.ac.uk (R.I. Todd).

https://doi.org/10.1016/j.ceramint.2024.11.314
Received 20 July 2024; Received in revised form 21 October 2024; Accepted 20 November 2024
Available online 21 November 2024

densification of B_4C by FS and is one of the aims of the present work.

This work also investigates the role of plasmas in FS and their effect on the densification during FS of non-oxides, focusing mainly on boron carbide. Saunders et al. [16] showed that the use of a high electric field (500 V/cm) and an argon atmosphere at atmospheric pressure could produce optical emissions from plasma generation when using conductive powders (ZrB_2, W). The use of lower fields did not generate plasmas, however, and although the effects of the plasma on powders were reported, there was no detailed investigation of the effect on sintering. More recent work on non-conducting oxide powders [17–20] has suggested that plasmas in the atmosphere around a powder compact (green body) can heat the sample to some extent, but no influence on sintering was apparent.

Part I of this work [21] showed that at elevated environmental temperatures of ≈1500 °C, a plasma can form around a bar shaped sample of B_4C or SiC mounted between two electrodes in Ar at atmospheric pressure if a DC electric field of 25 V/cm (50 V) or higher is suddenly applied. The atmospheric breakdown initially occurs by a flashover mechanism along the sample-atmosphere interface. During this "plasma pre-treatment" stage, sample heating was limited, and no significant densification took place but some ingress of the plasma into the green body was demonstrated by the transport of material from the interior of the sample, prepared by uniaxial pressing of a homogeneous powder consisting of B_4C and ZrO_2 marker material, to the surface. Typically, 15 s for B_4C and 240 s for SiC after the initial plasma formation, the materials' electrical conductance exceeded the conductance of the plasma, causing the plasma to collapse. All the subsequent current then passed through the sample and the resulting Joule heating raised the sample temperature to much higher temperatures, at which sintering occurred. This process was described as isothermal Plasma Pre-Treatment Flash Sintering (PPT-FS).

In some atmospheres such as He or N_2, no plasma formed under otherwise identical conditions to the experiments conducted in Ar, owing to the higher breakdown voltages (V_B) of these gases. This offers the potential to investigate the effects of the plasma on sintering by comparing FS with and without the plasma pre-treatment. The aims of the paper are therefore to identify any influence of the plasma pre-treatment and to establish conditions suitable for pressureless FS of B_4C to near full density for the first time. Relative densities, microstructures and hardness values for the ceramics produced are reported.

2. Materials and methods

2.1. Sample preparation

Boron Carbide (B_4C) powder (HD20, D_{50} = 0.3–0.6 μm, Höganäs) was used and samples were prepared as described in detail in Part I of this investigation [21]. The production of the bar-shaped green bodies (30 x 5 × 3 mm^3) included mixing of the primary powder with 1 wt% of PVB in ethanol. In some cases, a specified amount of carbon black (CB) ranging from 2 to 6 wt% was added under constant magnetic stirring and subsequent ball milling for 24 h. Slurries were dried in a rotary evaporator for at least 2 h, sieved (150 μm), and uniaxially and cold isostatically pressed to produce green bodies.

2.2. Flash sintering conditions

Debinding was conducted in argon (Ar, 99.998 % pure, <5 vpm O_2) at 600 °C for 1 h. An atmosphere-controlled horizontal alumina tube furnace was used for debinding, and FS, as described in Part I of the investigation [21]. Tungsten (W) electrodes were bent around a smaller alumina tube which was inserted into the furnace. Carbon paste was applied on both sides of the samples to reduce the contact resistance between the sample and the electrodes.

2.2.1. Constant voltage-constant power tests

Preliminary investigations of the electrical and thermal response of B_4C without added CB were conducted by applying constant electrical fields between 50 and 200 V/cm while heating the furnace with a heating rate of 600 °C/h from room temperature in Ar atmosphere. The field was applied from room temperature and a maximum power dissipation of up to 500 W (1.1 W/mm^3) was defined in the power-controlled stage after the transition from voltage to power control and held for 60 s before turning off the electrical field and furnace cool-down.

2.2.2. Isothermal flash sintering

If not stated otherwise, the electric field was applied in one step in Ar as soon as the furnace reached the defined temperature, which resulted in plasma formation prior to the Joule heating stage (PPT-FS) as described in the Introduction and Part I of the investigation [21]. Also for these default conditions, 4 wt% CB-containing B_4C-samples with C-foil thermal insulation were used at a furnace temperature of 1500 °C and a power of 700 W was dissipated for 5 min after initially applying 700 V (≈350 V/cm). For all experiments and samples shown in this work the cathode (−) was located on the right and anode (+) on the left side of the sample.

Departures from these standard isothermal PPT-FS conditions were used to investigate the effects of various parameters including power limit, the presence or absence of carbon foil around the sample for thermal insulation, carbon additive content, heating rate, suppression of plasma formation by changing atmospheric gas or electrical conditions, and hold time, as described in greater detail in the next paragraphs.

Power limits between 500 W (1.1 W/mm^3) and 800 W (1.8 W/mm^3) were used for the power-controlled stage, which affects the sample temperature during the Joule heating stage of (PPT-)FS. Sample temperature was estimated according to the black body radiation (BBR) model [22] and a constant emissivity (ε) of 0.85 was used for B_4C [23].

Carbon foil (C-Foil, 0.25 mm thick, 99.8 % (metals basis), Thermo Scientific Chemicals) was loosely wrapped around some samples to reduce heat loss by radiation from the sample surface and to improve heat distribution.

The effect of between 0 and 6 wt % *additional CB* was investigated, to enable carbothermal reduction of the B_2O_3-layer on the surface of the powder particles.

The influence of *heating rate* and *plasma formation* were investigated by various approaches.

I) PPT-FS as described in Ref. [21], where maximum power was applied from the very beginning of the experiment, conducted in argon (Ar).
II) Ramped FS in Ar, where power dissipation was increased stepwise at a rate of 50 W every 30 s up to the defined power limit.
III) FS in helium (FS-He), where the power limit is set to the maximum value from the beginning, but no plasma formed due to the higher breakdown resistance of He compared to Ar [21], enabling high heating rates without plasma formation to separate the influence of heating rate and plasma.

Hold times between 30 s and 30 min were applied from the point at which the maximum power dissipation in the power-controlled stage was reached. The plasma stage in PPT-FS, which lasts ≈15 s [16], is included in the applied hold times.

2.3. Characterisation

Relative density (RD) measurements were performed in water at room temperature based on the Archimedes principle using a theoretical density (TD) of 2.52 g/cm^3 for all samples and compositions.

Hardness measurements were performed in the centre of the cross section of the sample halfway between the electrodes at room temperature using a Future-Tech Corp. FV-110 Vickers hardness tester with an

applied load of 9.81 N (HV1) and calculated based on five indentations.

Raman Spectroscopy was conducted on polished cross sections of the sample at three different spots at room temperature using a Renishaw Raman microscope System 1000 with a 632.8 nm, 50 mW He-Ne laser.

Sample *imaging* was examined by FEG-SEM (Zeiss Merlin Germany), operating at an accelerating voltage between 1 and 10 kV, in the centre of the cross section of the sample halfway between the electrodes. The bulk samples investigated were prepared by sectioning, grinding, and polishing. Electrochemical etching (10 V for 30 s in 2.5 M NaOH solution) was used for some SEM samples and EBSD samples were ion polished. EDS was performed using a Bruker FlatQuad EDS detector. A Bruker QUANTAX EBSD-detector was used for EBSD characterisation and forescattered electron imaging (ARGUS™). Grain sizes were measured as the mean linear intercept (>100 intercepts per sample) using SEM images of etched microstructures and EBSD pattern quality images, which are not subject to the corrections involved in grain orientation software.

X-ray Photoelectron Spectroscopy (XPS) characterisation was performed on the sample surfaces to detect a potential plasma induced change in surface chemistry. XPS was conducted at room temperature using a PHIVersaprobe III XPS system generating focused, monochromatic Al Kα X-rays at 1486.6 eV, under ultrahigh vacuum (UHV) conditions with the main chamber maintained at pressures between $10^{-7} - 10^{-6}$ Pa. Gaussian-Lorentzian and Voigt line shapes were used to fit the elemental spectra after applying a Shirley background within CasaXPS software. Since some of the samples contained additional C and others did not, the C 1s signal, usually used as reference value in XPS, was not used. Instead, the B1s XPS-signal at 192.9 eV, referring to boron (B) in B_2O_3 [24], was used as reference value for all spectra, and the results verified using the corresponding O1s signal, located at a binding energy (BE) 139.3 eV higher than the B 1s signal for B_2O_3.

Treatments conducted and compared by XPS were:

I) green body made from pristine powder without any treatment (P),
II) pure B_4C green body heat treated at 1500 °C in Ar for 5 min (P-1500 °C),
III) same heat treatment for B_4C green body containing 4 wt% of additional C (P-C-1500 °C),
IV) 4 wt% C-containing green body subjected to Ar plasma treatment for 30 min in a low pressure plasma (cleaning) system/chamber (Tetra22 – Bell, Diener electronic GmbH & Co. KG, Germany), which is contained in an Ar-filled glove box at room temperature (P-C-PlCh),
V) surface of a 4 wt% C-containing B_4C powder compact, pre-plasma treated at 1500 °C (700 W) and stopped before the Ar plasma collapsed (P-C-PPT-Su),
VI) cross section of condition V) (P-C-PPT-CS),
VII) surface of a sample as for V) but after densification by PPT-FS conducted at a furnace temperature of 1500 °C, power limit 700 W, hold time 5 min with C-foil wrapping (D-PPT-FS-Su), and
VIII) cross section of condition VII) (D-PPT-FS-CS).

If powder compacts (P) were investigated, fractured cross sections (CS) were used. For dense, sintered (D) samples, ground and polished CS were characterised. A summary of the samples investigated by XPS can be found in Table 1.

To reduce the potential influence of reoxidation or other atmospheric reactions, the samples produced were transferred into an air-tight Ar-filled glove box (MB Braun, MB 200B) with O_2 and H_2O concentrations below 0.1 ppm, where all further preparation and mounting of the samples on the XPS sample holder was conducted. Transfer into the XPS without contact with air was possible.

3. Results

3.1. Constant voltage-constant power tests

Fig. 1 shows the electrical power dissipation against furnace temperature (Tf) with different applied electric fields whilst heating B4C green bodies at a rate of 600 °C/h in an Ar atmosphere. As with many FS systems, a rapid increase in power dissipation occurred beyond a specific furnace temperature, which decreased with increasing applied field ("runaway" [25–27]).

The initial rate of power increase at the critical temperature also increased with increasing field. Note that the initial sudden step up in power dissipation originates from the lowest current (0.06 A) detectable by the power supply multiplied by the applied voltage.

Although these results show that FS is possible in principle at furnace temperatures that are very low compared with the usual sintering temperature, current concentration and hot-spot formation resulted in inhomogeneous heating and local melting of the material as previously reported for FS of carbides by other researchers [8,9], even if the power dissipation limit was reduced to 100 W.

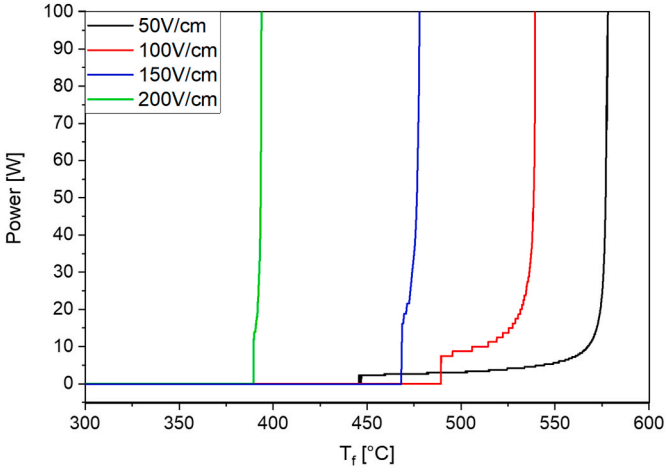

Fig. 1. Power dissipation and runaway behaviour in boron carbide (B_4C) at various field strengths between 50 and 200 V/cm dependent on the furnace temperature (T_f).

Table 1
Sample description and processing parameters for the samples investigated by XPS. P represents powder (compacts), prior to densification. Densified samples are labelled with D.

sample	atmospheric temp. [°C]	C-additive	plasma chamber	PPT	PPT-FS	surface	cross-section
P	20						
P-1500 °C	1500						
P-C-1500 °C	1500	X					
P-C-PlCh	20	X	X				
P-C-PPT-Su	1500	X		X		X	
P-C-PPT-CS	1500	X		X			X
D-C-PPT-FS-Su	1500	X			X	X	
D-C-PPT-FS-CS	1500	X			X		X

No plasma formation or other unusual phenomena occurred in these runaway experiments.

3.2. Isothermal flash sintering

Since the runaway experiments under constant electric field described above showed strong hot-spot formation, the effects of various processing parameters were investigated with isothermal flash sintering to improve densification of B_4C. This allowed FS to be conducted at a furnace temperature of 1500 °C, which was much higher than the runaway temperature in constant voltage experiments. This helped to avoid the localisation of heating.

3.2.1. Power dissipation limit

Power limits between 500 W and 800 W were applied during isothermal Plasma Pre-Treatment Flash Sintering (PPT-FS). Up to 700 W, density increased with power as shown in Fig. 2a. According to the BBR model a power dissipation of 700 W resulted in an estimated sample temperature of ≈2300 °C.

If a power dissipation of 800 W was applied, the contact regions between sample and electrode deteriorated significantly and the isothermal FS-experiment failed. This is consistent with the predicted temperatures, which approached the melting temperature of B_4C [23] under such conditions (≈2320 °C [28]).

3.2.2. C-foil wrapping

Fig. 3 shows 4 wt% C-containing B_4C-samples during the Joule heating stage of isothermal PPT-FS at 1500 °C and a power of 700 W without and with C-foil as thermal insulation.

In the latter case the straighter sample shape indicates a more homogeneous and improved densification of the sample, as is also confirmed by the density measurements, which indicated a RD increase by more than 7 %, (Fig. 2a). For this reason, the C-foil was used in the standard conditions.

Furthermore, the thermally insulating C-foil was significantly colder on the outside indicating that almost no current was flowing through the foil itself, which is confirmed by an equal conductivity with and without C-foil. Most of the heat generated within the sample was reflected back to it.

3.2.3. C-content

Fig. 2b shows that even for the PPT-FS specimens, which gave the highest densities, the addition of C is essential for successful sintering. For the range of additional C investigated, the maximum density was achieved for a C-content of 4 wt% after PPT-FS of B_4C and with thermal insulation (Fig. 2b). Note that residual C from thermal degradation of the 1 wt% PVB binder during debinding was not included in these values since it is difficult to specify how much C remained. If PVB is seen as $[C_8H_{14}O_2]_n$, the maximum residual C content from this source is 0.67 wt %.

According to the Raman spectroscopy results shown in Fig. 4, unreacted C residues were present if the additional C-content exceeded 2 wt%, particularly at the outside (O) of the cross-section. This is shown by the presence of the D- and G-Bands located at Raman shifts of ≈1350 and 1580 cm^{-1}, respectively. If the content exceeded 4 wt%, residual C could also be found in the cross-section halfway (M) between the sample centre (C) and the outside (O).

Beside the D- and G-Bands of unreacted C, all the major peaks in the Raman spectra can be associated with B_4C [29]. In particular, the well-defined and narrow Raman peaks at 481 and 534 cm^{-1} are representative for B_4C with a well-ordered C-B-C chain in the stoichiometric B_4C-crystal containing 20 at% C [30].

3.2.4. Heating rate and initial presence of plasma

The heating rate with the PPT could not be varied in isolation because the switch from electrical conduction through the plasma, with minimal sample heating, to conduction through the sample, resulting in rapid Joule heating to the sintering temperature, depended on the

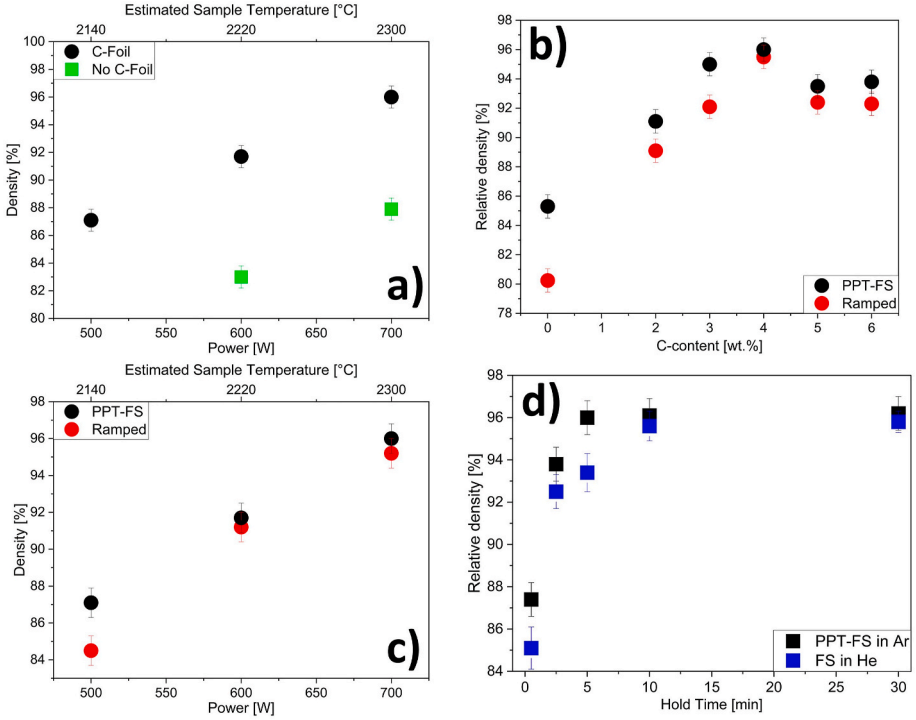

Fig. 2. Measured relative density of (PPT-)FS B4C dependent on a) presence of thermal insulation and power dissipation during PPT-FS with the estimated sample temperature shown on the top X-axis (estimated according to Ref. [22] without consideration of the thermal insulation); b) different heating approaches in Ar (PPT-FS or ramped) and C-content; c) heating approach in Ar and power dissipation; d) PPT-FS in Ar or FS in He and hold times between 30 s and 30 min after the application of maximum power (700 W). The standard conditions in section 2.2.2 were used for unspecified experimental variables.

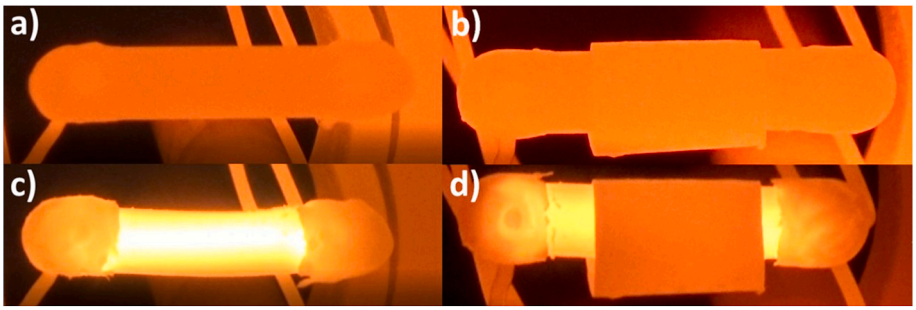

Fig. 3. B_4C sample before and during the FS stage of PPT-FS, without (a and c) and with (b and d) a C-foil wrapped around the sample for reduction of heat loss by thermal radiation from the sample surface.

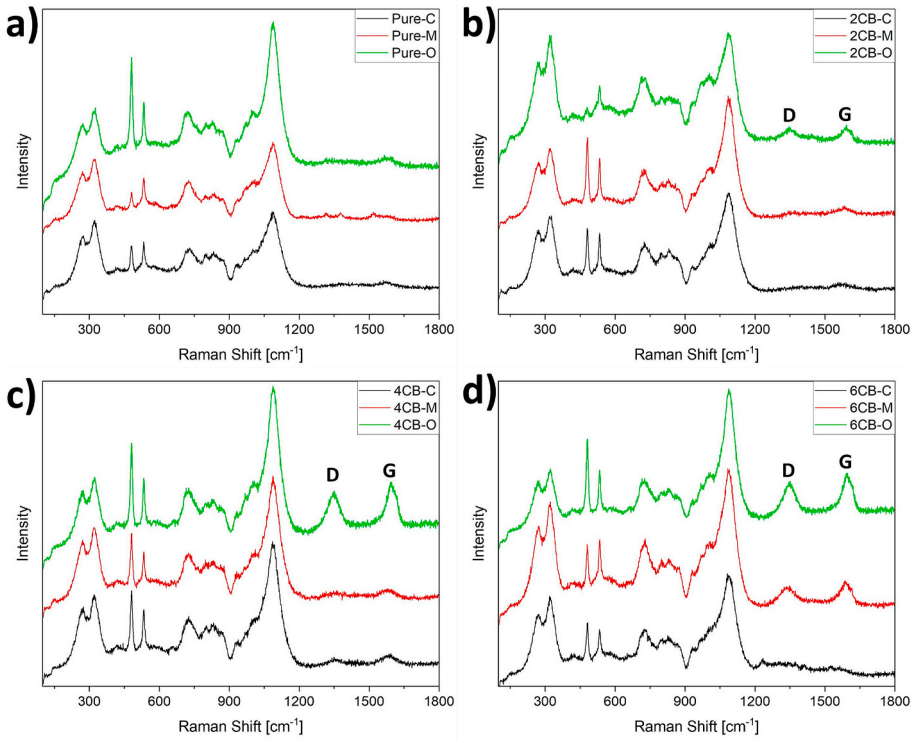

Fig. 4. Raman spectra taken from the centre (C), between the centre and the outside (M), and outside (O) of PPT-FS B4C cross sections with a) no additional carbon black (CB); b) 2 wt% CB, c) 4 wt% CB and d) 6 wt% CB. Residual CB can be observed in the D and G bands at Raman Shifts of ≈1350 and 1580 cm^{-1}.

properties of the plasma and the sample rather than directly controllable experimental variables.

However, the results for the power ramped samples and FS-He samples in Fig. 2b and d allow a comparison between different heating rates in the absence of the PPT, because the gradual increase in power in the ramped tests avoided the initial formation of plasma and the high breakdown strength of He prevented plasma formation in the FS-He samples. However, the ramped samples took up to 7 min to reach the maximum temperature under electrical heating, whereas the FS-He samples took only a few seconds [21]. The 4 % C ramped result in Fig. 2b and the 5 min FS-He result in Fig. 2d were obtained under the same conditions apart from the heating rate (and inert gas in the atmosphere) and the ramped sample had a slightly higher RD (95.4 %) than the much more rapidly heated FS-He sample (93.3 %).

The plasma-free FS-He samples, which experienced comparable heating rates to those for PPT-FS in Ar as shown in Ref. [21], displayed a significantly lower RD for all applied hold times (Fig. 2d), showing that the PPT was beneficial to sintering. All PPT-FS samples also gave higher densities than the slowly heated ramped samples for all C contents and power levels (Fig. 2b–c). The difference was stronger at shorter hold times, particularly up to a hold time of 5 min.

3.2.5. Hold time

A significant increase in RD for PPT-FS in Ar was seen as hold time increased up to 5 min (Fig. 2d). Since longer hold times could lead to sample or setup failure and material degradation but did not yield an improvement in density, 5 min hold time was determined as ideal. The FS-He samples without plasma formation took twice as long as this to reach their maximum density.

Based on the above results, the ideal FS conditions for B_4C are 1500 °C T_f, instantaneous application of maximum electric field in Ar to form a plasma (PPT-FS), power dissipation of 700 W, 4 wt% carbon additives, 5 min hold time, and C-foil wrapped around the sample for thermal insulation.

3.3. Hardness

If the optimum conditions (PPT-FS in Ar at 1500 °C, 700 W power

dissipation, 5 min hold time, 4 wt% additional C, and thermal insulation) were applied so that a sample density of 96 % was achieved, a hardness HV1 of 31.0 ± 0.2 GPa was measured.

3.4. Microstructure

3.4.1. PPT-FS samples

SEM images of a fractured cross section of a 96 % dense B_4C sample processed under the optimum conditions can be seen in Fig. 5 at various magnifications. The majority of the pores are located along the grain boundaries with a minor number of intra-granular pores (Fig. 5b). Some of the pores are filled with unreacted carbon, confirmed by EDS and highlighted with a white arrow in Fig. 5c.

Microstructures of the centres of polished PPT-FS B_4C densified to 87 % and 96 % RD are shown in Fig. 6a and Fig. 6b, respectively. The SEM images show that small pores disappear during densification, whereas the bigger pores in the range of several μm coarsen and remain. This can also be seen in the SEM images showing the 96 % dense microstructure at various other magnifications (Fig. 6c–e). As already mentioned for the fractured cross section shown in Fig. 5, some of the bigger pores contained unreacted carbon. This can be seen by the fine carbon structures, also confirmed by EDS, contained in the big ~25 μm pore shown in Fig. 6f. SEM images of other regions of the 96 % RD PPT-FS sample (Fig. S1) show that the density first decreases slightly in moving outwards from the centre, which is usual for flash sintering because of the through-thickness temperature gradient. However, there is also a dense layer of up to 0.5 mm thickness at the surface, which is unusual in conventional FS.

To reveal the grains, an EBSD-pattern quality map and a fore-scattered electron image of 96 % dense PPT-FS B_4C can be seen in Fig. 6g and h. The grain size in the centre of the sample was 8.2 ± 0.6 μm and almost all grains show several well-defined twins.

3.4.2. Plasma-free samples

The FS-He 93 % dense microstructure produced under otherwise standard conditions (Fig. S2) shows a bimodal pore distribution, including the several micrometre intergranular pores present in the PPT-FS samples but also a greater population of submicron intragranular pores.

The plasma-free samples also had larger grain sizes than the corresponding PPT-FS samples, particularly for the power-ramped samples, as is summarised in Table 2.

3.5. Influence of plasma on boron carbide particles

According to the results in Section 3.2.5, a pre-treatment plasma stage prior to Joule heating is beneficial for the densification of B_4C. The effects and the influence of plasma on the microstructure and surface chemistry of the B_4C are investigated in the following section.

3.5.1. Plasma induced change in surface morphology

The morphology and structure of B_4C particles before and after the pre-treatment plasma stage in Ar, which was stopped after a plasma formation of 12 s, just before the plasma collapsed according to the previous investigation [21], is shown in Fig. 7.

The particles before the plasma treatment (Fig. 7a and d) show a rather smooth surface. After the plasma treatment the particles in the centre of the sample cross section (Fig. 7b and e) show a slightly roughened surface, and this surface roughening is much more pronounced for particles near the surface of the B_4C-sample (Fig. 7c and f). For clarity, enlarged images of Fig. 7d) and e) are shown in Figs. S3 and S4. No sign of densification was observed in this stage of PPT-FS.

3.5.2. Plasma induced change in surface chemistry

Fig. 8a shows the XPS survey scan for each of the samples in a BE range between 0 and 1050 eV. Some significant differences can be observed. The most important are shown in separate graphs as follows.

Fig. 8b shows the core-level spectra for B 1s in more detail for all samples, showing two different peaks around 187.5 eV and 193 eV. The peak near 187.5 eV can be deconvoluted into two single peaks representing two different kinds of bonding interactions as will be elaborated later.

Fig. 8c shows the core-level spectra for C 1s suggesting the presence of multiple peaks. Samples P-C-PPT-Su and D-PPT-FS-Su (sample nomenclature is summarised in Table 1) show the most intense signal in this range.

The O 1s spectrum as depicted in Fig. 8d is most intense for the pristine powder (P), followed by that for the heat-treated powder compact without additional C (P-1500 °C). The least intense O 1s spectra was obtained in the middle of the dense flash sintered sample (D-PPT-FS-CS). Since some samples are less dense than others and the flatness of the characterised surface varies, direct comparison of the spectra from one sample to another should be treated with caution. However, the spectra provide a basis for binding environment for different elemental species and their quantification within the same sample.

From the B 1s spectra the potential presence of B_2O_3 can be inferred from the peaks obtained at BE characteristic of B-O bonds, and of boron carbide (B_4C) from peaks characteristic of B-C and B-B bonds. The deconvoluted B 1s XPS spectra in Fig. 9 show that the pristine powder (Fig. 9a) contained predominately B-O bonds, whereas, for dense samples after PPT-FS the peak characteristic of B-O is less intense and barely present at all in the cross-section (D-PPT-FS-CS).

To highlight the changing ratio of B_2O_3 to B_4C, the peak area ratio of the B-O peak (blue area in Fig. 9) to the combined B-B/B-C peak (green and red area in Fig. 9) was calculated and is shown in Fig. 10. Based on the XPS-results, a ratio of 10 is calculated for the pristine powder (P). If no C was added and the green body powder compact was heated to 1500 °C in Ar (99.998 % pure), this ratio increased by almost 10 times (P-1500 °C), whilst in the presence of additional C it remained almost the same (P-C-1500 °C). After a plasma cleaning treatment at room temperature for 30 min, the ratio decreased by 80 % (P-C-PlCh) and

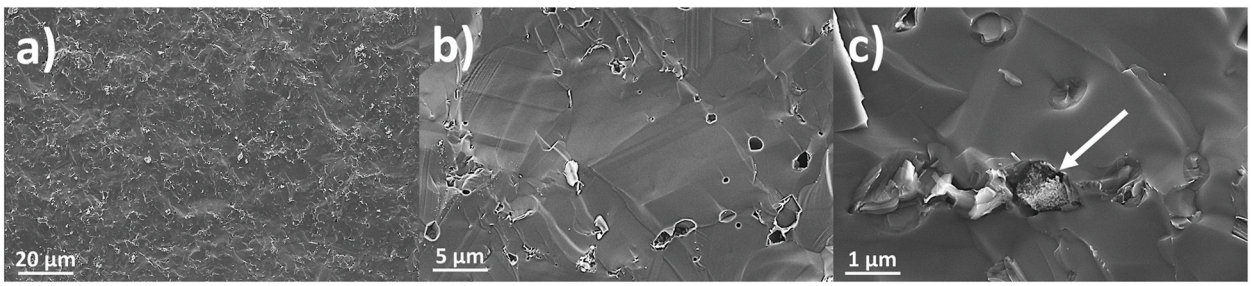

Fig. 5. SEM images at various magnifications of a fractured cross section of a 96 % dense B_4C sample containing 4 wt% additional carbon, densified by PPT-FS for 5 min at 1500 °C T_f under a power dissipation of 700 W including thermal insulation; a) shows the overall fractured microstructure; b) a more detailed section showing the major porosity along the grain boundaries with some minor intragranular porosity; c) shows unreacted carbon within the B_4C matrix.

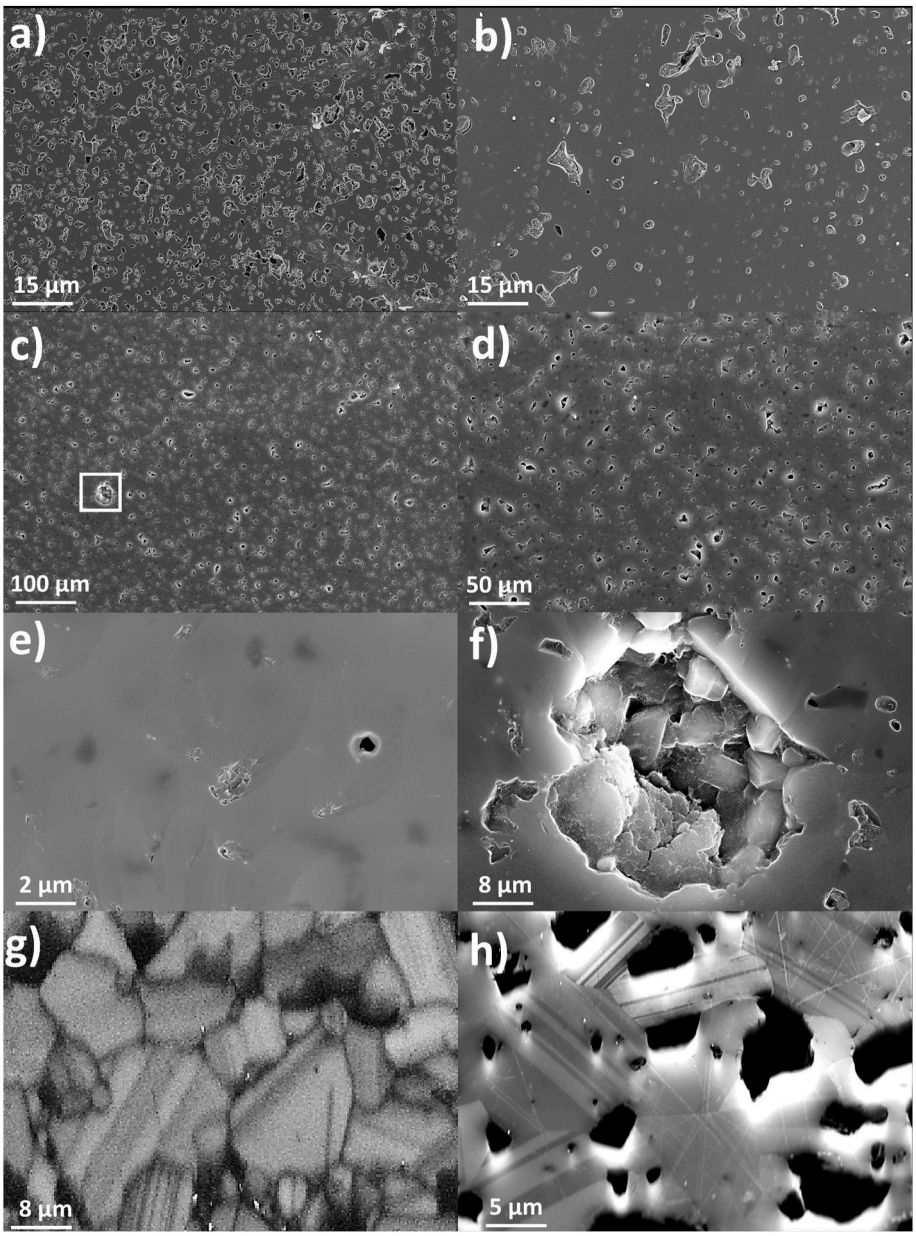

Fig. 6. Microstructures of the polished cross sections of: a) 87 % dense and b) 96 % dense thermally insulated PPT-FS B_4C-samples containing 4 wt% C, densified at 1500 °C T_f for 5 min by power dissipation of 500 W and 700 W respectively; c)-e) show the 96 % dense polished microstructure at various magnifications; f) shows a more macroscopic pore which is highlighted in c); g) EBSD-pattern quality map visualising grain structure and twinning; h) shows a forescattered electron image of the microstructure, including some non-diffracting regions (black).

Table 2
Grain sizes produced and relative density resulting from different flash sintering conditions. All other experimental variables were the defaults described in section 2.2.2.

FS conditions	RD (%)	grain size (µm)
PPT-FS	96	8.2 ± 0.6
FS-He	93	10.1 ± 0.5
Ramped power	95	14.8 ± 0.7

decreased even more if treated by the plasma during the pre-plasma stage of FS (P-C-PPT-Su and -CS). The lowest ratios were in the PPT-FS samples, especially the cross section (D-PPT-FS-CS), which had a ratio of 0.05.

4. Discussion

4.1. Boron carbide runaway behaviour at low furnace temperatures

B_4C is a semiconducting material with a bandgap of 2.09 eV [29, 31–33]. Thus, it is not surprising that the B_4C green bodies subjected to moderate temperature and electric field were able to exhibit a rapidly increasing current. This thermal runaway is associated with the NTC resistivity expected of a semiconductor [25,27]. However, when combined with the temperature gradients associated with radiative heat loss from the surface of the electrically heated sample to the cooler furnace atmosphere [25,34–36], such conditions are also known to lead to the current concentration in the sample centre observed here and by Rosenberger et al. [9], such that uniform densification cannot be achieved. The more severe localisation seen by Rosenberger et al. [9] may be a consequence of their thicker samples and low furnace temperatures on

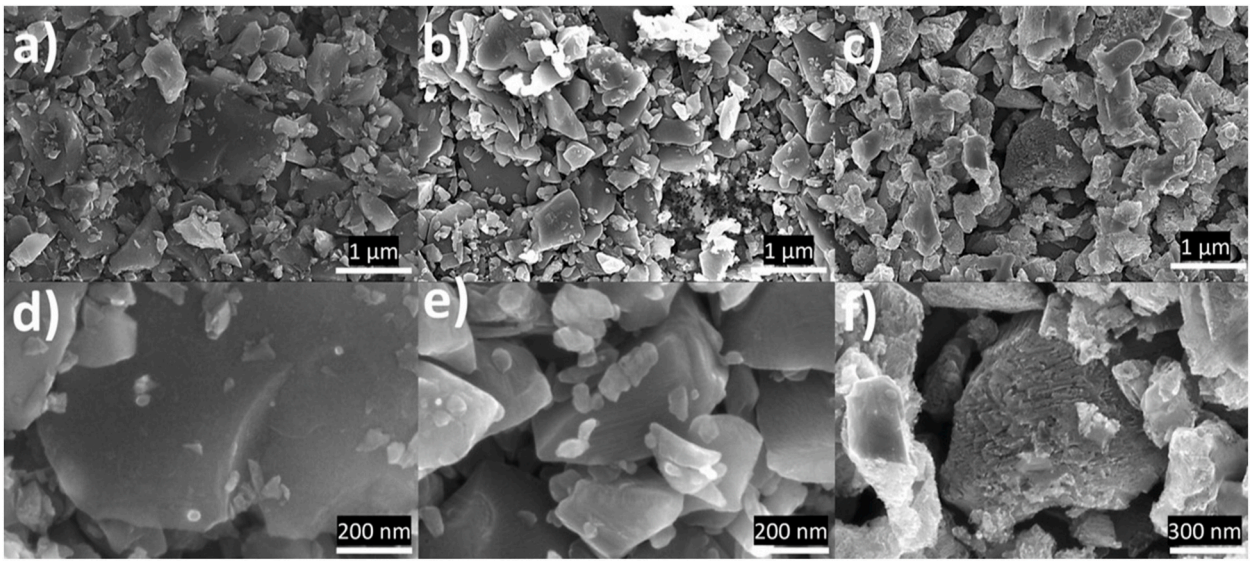

Fig. 7. Boron carbide particles before (a and d) and after plasma pre-treatment stage during PPT-FS; b) and e) show particles in the cross section of the sample; c) and f) on the surface.

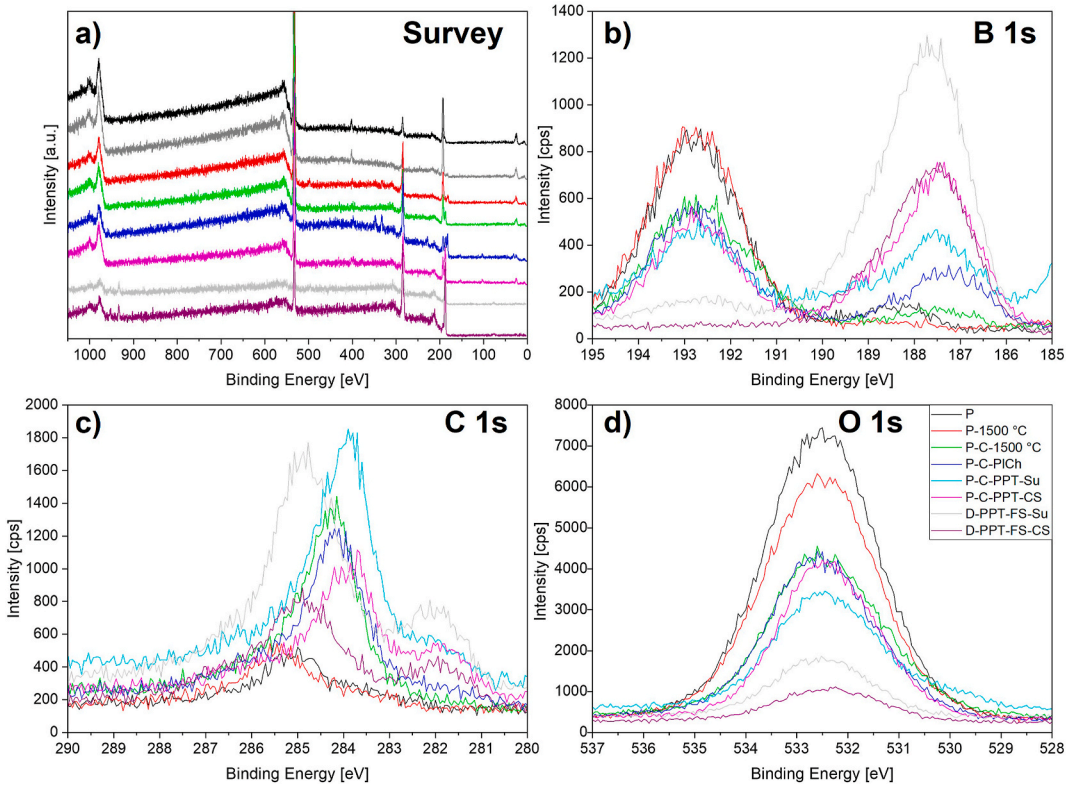

Fig. 8. a) XPS Survey; b) B 1s; c) C 1s and d) O 1s region of the XPS signal of various B_4C samples with and without plasma and heat treatments. The legend applies to all panels.

this basis. Other factors such as improving particle-particle-contacts during densification, and the removal or breakdown of oxide layers between the particles, can also be the origin of current localisation in carbides. In contrast, electrochemical reduction, which is known to influence current localisation during FS of oxide ceramics such as YSZ [37,38], is not known to such an extent in carbides, and is therefore a less important factor in FS of SiC and B_4C.

The results are also consistent with previous work on SiC which has a higher bandgap between 2.3 and 3.3 eV [39,40] depending on its phase. SiC shows a rapid increase in current around ≈800 °C if a field of 40 V/cm is applied [8], which is ≈ 200 °C higher than observed here for B_4C. As in our results on B_4C, attempts to FS SiC [8] with a low furnace temperature (1032 °C) also resulted in insufficient overall densification of the material (78 %).

We conclude that there is an inherent limitation in using FS for semiconducting carbides at low environmental temperatures (<1000 °C) because the great difference with the temperature required for sintering such ceramics (>2000 °C) leads to high temperature

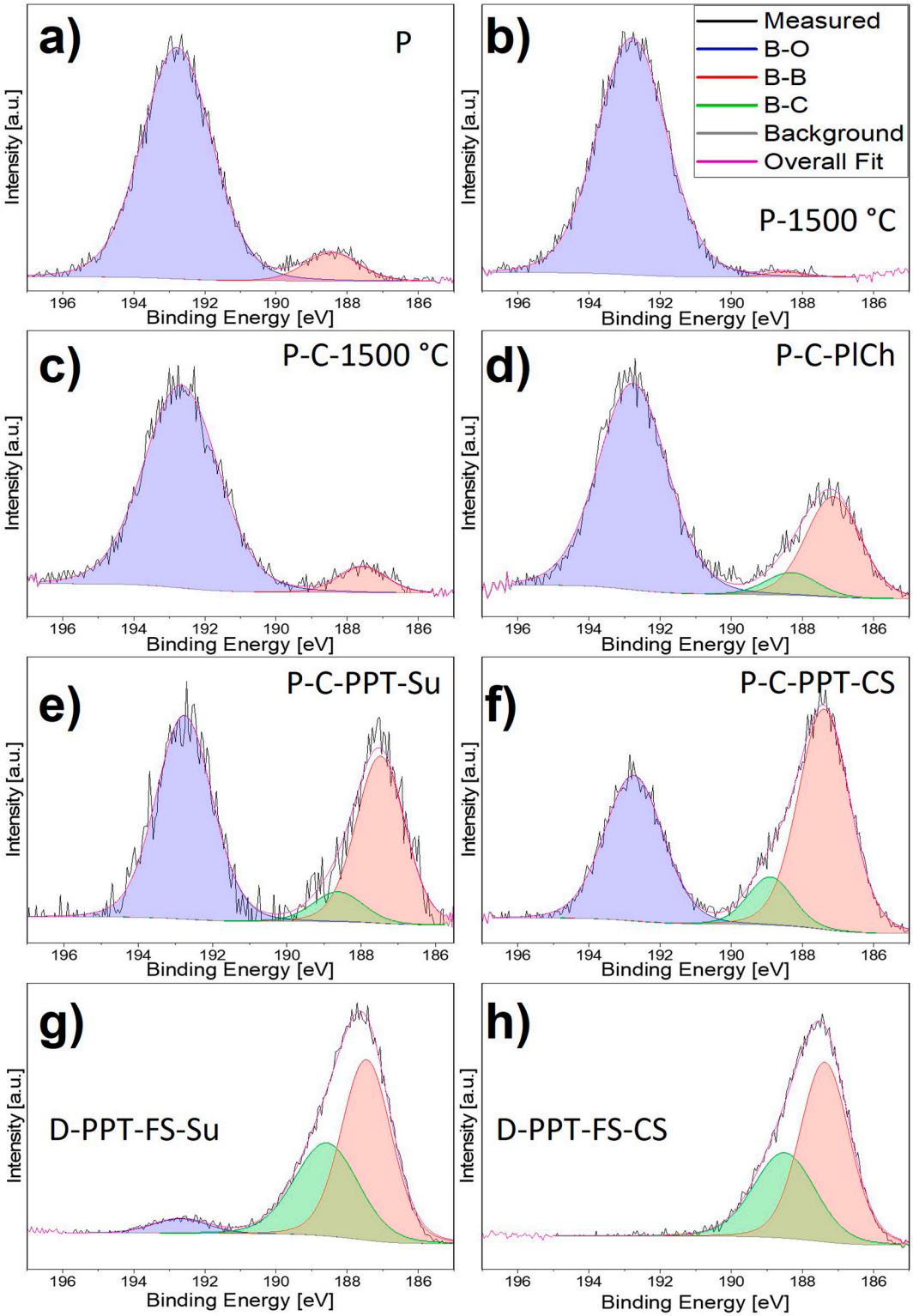

Fig. 9. B 1s region of the XPS spectra taken from samples treated in various ways prior to the characterisation. The B 1s is deconvoluted into B-O (blue), B-B (red) and B-C bonds (green). The legend applies to all panels. (For interpretation of the references to colour in this figure legend, the reader is referred to the Web version of this article.)

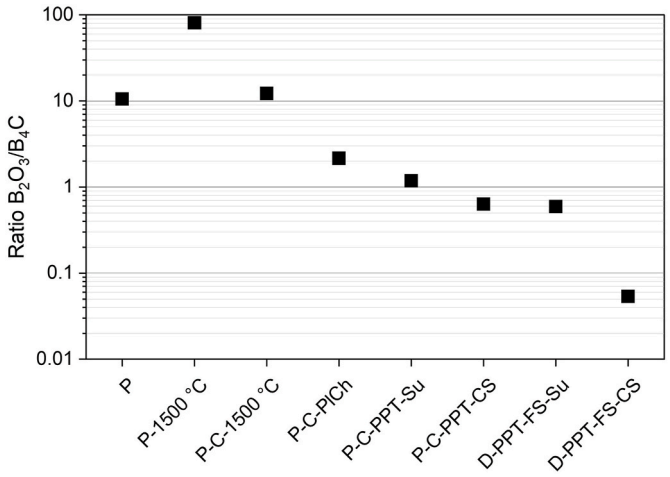

Fig. 10. B_2O_3 to B_4C ratio of various samples calculated based on the deconvoluted B 1s XPS signal.

gradients between the centre of the cross-section and the edges, which are exacerbated by localisation of the current.

4.2. Factors Affecting sintered density

4.2.1. Specimen heating: influence of furnace temperature and C-foil insulation

The use of a higher furnace temperature (1500 °C) in isothermal FS was successful in suppressing localisation of the heating sufficiently for high densities to be achieved. This is also consistent with previous work on FS of SiC [8]. This furnace temperature is 700–800 °C below the temperature for conventional sintering of these carbides and allows the use of less expensive equipment, saves a substantial amount of energy, and leads to significantly shorter heating and cooling times.

The presence of the C-foil is also beneficial to RD (Fig. 2a). At such high temperatures, radiation is the primary mechanism of heat loss and the relatively low temperature of the foil apparent in Fig. 3d indicates both that the foil is not acting as a short circuit for the current and also that it was effective in reflecting much of the thermal radiation from the sample back towards it. Not only did this reduction in surface heat loss lead to more uniform heating, as noted in Section 3.2.2, but also it would increase the specimen temperature for a given power, enabling better sintering without degradation of the electrodes (Section 3.2.1). This improvement of densification with thermal insulation agrees with previous work on FS of 8YSZ [41].

In the situation where the small amount of oxygen in the flowing Ar atmosphere, or oxygen diffusion through the alumina tube, is able to oxidise the B_4C, as is discussed in more detail in section 4.2.3, an additional benefit of the wrapping may be a further suppression of the oxidation, by shielding the sample from direct impingement of the flowing Ar and reduction of atmospheric oxygen, as suggested in a previous work [14], where the presence of solid carbon in the vicinity of SiC samples flash sintering in Ar was found to be critical in optimising the density. Given the presence of several other controls on oxidation, however, we suggest that the main benefit of the wrapping on sintered density seen in Fig. 2a is through its intended purpose of thermal management.

4.2.2. B_2O_3 I: effect of heating rate and C additions

The use of C additives in sintering B_4C is well known but one factor that distinguishes FS from conventional sintering is the high sample heating rate. The variation of the electrical results in part I [21] shows that the final stage of heating from close to the furnace temperature of 1500 °C to the sample sintering temperature of ~2300 °C occurs over a similar time scale of ~3 s for both FS in He and PPT-FS in Ar, with the only difference being the pre-plasma stage in PPT-FS, during which sample heating was limited. This gives an estimated heating rate of up to 270 °C/s, or 16000 °C/min. The ramped sample heating rates were much slower at ~150 °C/min.

The findings of Dole et al. [13,42,43] provide a useful starting point for the discussion of the effect of heating rate and C-addition. These authors found that the main problem with conventional sintering of undoped B_4C is that the presence of B_2O_3 on the surface of the powder particles leads to rapid coarsening in a temperature range around 1800 °C, which subsequently prevents the attainment of high density when the sintering temperature (2250–2300 °C) is reached. Two solutions were investigated. The first was to increase the heating rate used from 30 °C/min to ≈300 °C/min [13]. This minimised the time spent in the coarsening temperature range and enabled densities of up to 90 % to be achieved, though coarsening still prevented the attainment of higher densities. All the PPT-FS and FS-He results in this work, with their even higher heating rates should also have benefitted from this “fast firing”, which is also well known in other ceramics, in which different low temperature coarsening mechanisms can operate [44–49]. However, Fig. 2b shows that even with their very high heating rate, the PPT-FS results for samples with no added C only reached 85 % RD, so as for the results of Dole et al., any effect of high heating rate on its own was limited.

Taken at face value, the comparison of the power ramped and FS-He samples with otherwise identical sintering parameters (section 3.2.4) suggests that in fact slower heating is advantageous, at least in the absence of a plasma. However, the ramped samples spent much longer at high temperature than the FS-He samples owing to their slow heating rate and is the probable reason for their slightly higher sintered density. Though “slow” in the context of the present work, the ramped heating rate of 150 °C/min is towards the higher end of those investigated by Dole et al. and while the grain size was higher than for the FS-He samples (Table 2), the heating rate was evidently sufficient to avoid the worst effects of coarsening during heating.

The other, more effective solution to the coarsening problem advocated by Dole et al. was to remove the B_2O_3 by adding C to carbothermally reduce it. This was also effective in our work and a reduction of B_2O_3 content by almost an order of magnitude of powders heated to 1500 °C on adding C was confirmed by XPS (Fig. 10). The optimum amount of 4 wt% C is similar to previous reports of conventional pressureless sintering of B_4C [10–12,50–52], as is the observation of unreacted, C-filled porosity, even with the optimum C content (Fig. 6) [13,43]. This is a consequence of the difficulty in dispersing the CB homogeneously. However, the higher C content nearer the surface (Fig. 4) is peculiar to FS and is attributed to the lower temperature there due to heat loss from the surface and possibly to the increased plasma activity near the surface, as is discussed in section 4.2.3. The observed increase in C throughout the specimen beyond the optimum amount required to remove the B_2O_3 is presumably responsible for the accompanying decrease in sintered density.

4.2.3. B_2O_3 II: effect of plasma

The PPT-FS method developed in the present work adds a further solution to the B_2O_3 problem: removal by plasma treatment. Plasma pretreatment at 1500 °C reduced the B_2O_3 content by a further order of magnitude compared with a carbon-containing green body (Fig. 10) and led to clear improvements in subsequent sintering under all conditions (Fig. 2b–d). It is notable that the lowest B_2O_3 content of all investigated samples is detected in the interior of the fully PPT-FS B_4C which supports the assumption of the plasma induced elimination of the B_2O_3.

This treatment was more effective in removing the B_2O_3 than the commercial plasma cleaner applied at room temperature (P-C-PlCh, Fig. 10) and importantly, removed it immediately before heating to the sintering temperature on the collapse of the plasma. The significance of this is that simply heating the powder to 1500 °C in Ar led to nearly an order of magnitude increase in oxide (Fig. 10), so the efficacy of room

temperature pre-treatments in improving sintered density is expected to be limited. The continual oxidation of the B_4C particles during sintering may be the reason that C additions are still required for high densities to be achieved (Fig. 2b).

The additional benefits of the plasma pre-treatment enabled a RD of 96 % to be achieved with a hold time of only 5 min at a nominal sample temperature of 2300 °C. For comparison, the FS-He samples in Fig. 2d required 10 min to attain their slightly inferior maximum density, and the similar maximum RD of 97 % achieved using conventional heating at the same temperature in Ref. [13] used a much longer hold time of 30 min.

A comparison of the grain sizes for the PPT-FS and FS-He samples in Table 2 confirms that part of the advantage in removing the B_2O_3 immediately prior to densification was that the grain size was almost 25 % larger without the PPT, as expected from the work of Dole et al. [13]. In addition, the FS-He microstructure in Fig. S2 includes many submicron intragranular pores, which were not seen to such an extent in PPT-FS B_4C. Dole et al. also suggested that the presence of intragranular pores can be explained by evaporation and trapping of B_2O_3 from the surfaces of the powder particles during rapid densification, adding a further benefit from its removal before sintering.

The removal of oxide layers by similar plasmas is well known [53,54]. One established example is the cleaning and etching process of silicon (Si) wafers to reduce the oxidised layer of the material and improve its properties for further processing steps. In the context of sintering, a potential cleaning effect by a plasma was also suggested during (F)SPS of ZrB_2 and W [16]. Part I of this work [21] demonstrated the ability of the plasma pre-treatment to sputter marker material (zirconia) from within the powder compact, which was not seen during FS in He, i.e. without the initial plasma formation under otherwise comparable circumstances, and the same process is presumed to be responsible for the removal of the B_2O_3. Indeed, the etching of the particle surfaces by the plasma is evident in Fig. 7, S3 and S4. The fact that the etching is more pronounced near the surface than in the centre of the green body supports the conclusion made in Part I [21] that the plasma cannot be sustained independently within the green body because the pores are too small to allow sufficient acceleration of the electrons. Instead, charged particles must enter the green body from the external plasma around it, explaining the maximum etching near the surface. The effect of a higher plasma activity and removal of B_2O_3 near the surface of the sample is also the most likely reason for the dense layer on the outside of the sample after PPT-FS, as shown in Fig. S1. It may also contribute to the high C levels near the surface of the sintered sample, as the removal of B_2O_3 by the plasma would prevent it from reacting with the C additive.

4.3. Hardness of PPT-FS boron carbide

The grain size of 8 μm for the optimum conditions is at the upper end of the range reported in the literature for B_4C pressurelessly sintered to similar densities with C as a sintering aid [55]. This indicates that the rapid sintering in PPT-FS of C-doped B_4C is accompanied by equally rapid grain growth so that finer grain sizes than are possible with conventional sintering are not produced.

Nonetheless, our hardness (HV1) of 31 GPa for the 96 % dense samples is exceptionally high for B_4C pressurelessly sintered with carbon as the sintering additive. Zorzi et al. [56], for example, report a value of only 19.3 GPa for 1 kg Knoop hardness of B_4C-4%C pressurelessly sintered to 97.7 % dense. It is difficult to establish the reasons in this case because no microstructural information is available in Ref. [56]. Roy et al. [57] used similar additives to this investigation and achieved a hardness (HK100) of 24–25 GPa for a 90 % dense pressurelessly sintered sample, which is also hard to compare due to the significantly lower density, missing grain size and difference in hardness testing procedure.

Gubarevich et al. [58] achieved a hardness (HV3-10) of 30 GPa for ≈ 95 % dense B_4C without additives and a grain size ranging from 3.7 to 10.3 μm, which is comparable to the values achieved here. The material in Ref. [58] was densified via rapid pressureless densification with electromagnetic induction assistance, another method of rapid heating.

It should be noted that similar hardness values to ours have been reported in pressurelessly sintered B_4C with other additives [55,59–62], but some of these hardness tests were performed by micro- or nano-testing in which the significantly lower loads would give a higher hardness because of the indentation size effect.

A reliable comparison using the same indentation load as ours with SPSed material is available, however. Moshtaghioun et al. [63] found a similar hardness to ours of HV1 = 33 GPa for 99.2 % RD B_4C with a grain size of 17 μm. Moshtaghioun et al. [63] argue that the twin spacing may give a better indication of Hall-Petch-type hardening than the grain size. The ability of the PPT-FS process to produce such hard material may therefore be related to the twinning observed in Fig. 6. Twinning is known to develop mainly at low temperature and to anneal out at high temperature [64] and is common in B_4C because of its low stacking fault energy [65–68]. The short sintering times with PPT-FS, SPS and the induction assisted rapid heating method of Gubarevich et al. [58] may enable the twinning, and the increased hardness that accompanies it, to be retained to a greater extent than in slow, conventional sintering where it may have time to anneal out. However, this matter needs further investigation.

5. Conclusions

DC-Flash sintering of boron carbide (B_4C) was investigated under various conditions, revealing that high environmental temperatures of 1500 °C are necessary for uniform densification due to strong current concentration at lower furnace temperatures.

The application of high electric fields in an Ar atmosphere led to the formation of a plasma around the specimen. SEM and XPS results are consistent with the finding of Part I [21] that the Ar-plasma can enter the green body and show that it interacts with the solid particles, the strongest interaction being near the sample surface.

The plasma did not cause significant densification itself, but was shown to significantly reduce the oxide layer on the particle surfaces and thereby to enhance the subsequent densification of the material when the plasma collapsed and Joule heating raised the sample temperature to ~2300 °C.

The use of this Plasma Pre-Treatment-Flash Sintering process with carbon sintering aids and optimised process parameters enabled B_4C with density, grain size and hardness of 96 %, 10 μm and 31 GPa (HV1) to be produced by flash sintering without the application of pressure, using a furnace temperature of 1500 °C and a hold time of only 5 min. This represents the first successful pressureless flash sintering of B_4C.

CRediT authorship contribution statement

Christian Bechteler: Writing – review & editing, Writing – original draft, Visualization, Validation, Project administration, Methodology, Investigation, Formal analysis, Data curation, Conceptualization. **Sudarshan Narayanan:** Writing – review & editing, Methodology, Investigation, Formal analysis. **Richard I. Todd:** Writing – review & editing, Writing – original draft, Supervision, Resources, Project administration, Methodology, Funding acquisition, Conceptualization.

Declaration of competing interest

The authors declare the following financial interests/personal relationships which may be considered as potential competing interests: Richard I Todd reports equipment, drugs, or supplies was provided by EPSRC. Christian Bechteler reports financial support and equipment, drugs, or supplies were provided by EPSRC. Christian Bechteler reports financial support was provided by Studienstiftung des deutschen Volkes. If there are other authors, they declare that they have no known

competing financial interests or personal relationships that could have appeared to influence the work reported in this paper.

Acknowledgements

This work was supported by the Engineering and Physical Sciences Research Council [EP/T517811/1] and the Studienstiftung des deutschen Volkes – German Academic Scholarship Foundation.

The authors acknowledge use of characterisation facilities within the David Cockayne Centre for Electron Microscopy, Department of Materials, University of Oxford, alongside financial support provided by the Henry Royce Institute (Grant ref EP/R010145/1).

We also wish to acknowledge the support of the Henry Royce Institute for advanced materials for C.B. through the Student Equipment Access Scheme enabling access to XPS facilities at University of Oxford; EPSRC Grant Number EP/R00661X/1).

Appendix A. Supplementary data

Supplementary data to this article can be found online at https://doi.org/10.1016/j.ceramint.2024.11.314.

References

[1] A.L. Duval D'Adrian, Article of Fused Metallic Oxide and Process of Producing the Same, Oct. 03, 1922 1430724.
[2] M. Cologna, B. Rashkova, R. Raj, Flash sintering of nanograin zirconia in 5 s at 850°C, J. Am. Ceram. Soc. 93 (11) (2010) 3556–3559, https://doi.org/10.1111/j.1551-2916.2010.04089.x.
[3] E.A. Olevsky, S.M. Rolfing, A.L. Maximenko, Flash (Ultra-Rapid) spark-plasma sintering of silicon carbide, Sci. Rep. 6 (2016) 33408, https://doi.org/10.1038/srep33408.
[4] H. Li, G. He, N. Lu, J. Li, Flash spark plasma sintering of Zr1−xTixC solid solution, J. Ceram. Soc. Jpn. 129 (9) (Sep. 2021) 21045, https://doi.org/10.2109/jcersj2.21045.
[5] S. Grasso, T. Saunders, H. Porwal, B. Milsom, A. Tudball, M. Reece, Flash spark plasma sintering (FSPS) of alpha and beta SiC, J. Am. Ceram. Soc. 99 (5) (2016) 1534–1543, https://doi.org/10.1111/jace.14158.
[6] B. Niu, F. Zhang, J. Zhang, W. Ji, W. Wang, Z. Fu, Ultra-fast densification of boron carbide by flash spark plasma sintering, Scripta Mater. 116 (2016) 127–130, https://doi.org/10.1016/j.scriptamat.2016.02.012.
[7] E. Zapata-Solvas, S. Bonilla, P.R. Wilshaw, R.I. Todd, Preliminary investigation of flash sintering of SiC, J. Eur. Ceram. Soc. 33 (13–14) (2013) 2811–2816, https://doi.org/10.1016/j.jeurceramsoc.2013.04.023.
[8] A. Gibson, Y. Li, R.S. Bonilla, R.I. Todd, Pressureless flash sintering of α-SiC: electrical characteristics and densification, Acta Mater. 241 (Dec. 2022) 118362, https://doi.org/10.1016/J.ACTAMAT.2022.118362.
[9] A. Rosenberger, R.E. Brennan, A.L. Fry, Flash sintering feasibility study and localized densification in boron carbide, J. Am. Ceram. Soc. 104 (8) (Aug. 2021) 3823–3827, https://doi.org/10.1111/jace.17833.
[10] H. Lee, R.F. Speyer, Pressureless sintering of boron carbide, J. Am. Ceram. Soc. 86 (9) (2003) 1468–1473, https://doi.org/10.1111/j.1151-2916.2003.tb03498.x.
[11] H. Lee, R.F. Speyer, Hardness and fracture toughness of pressureless-sintered boron carbide (B4C), J. Am. Ceram. Soc. 85 (5) (2002) 1291–1293, https://doi.org/10.1111/j.1151-2916.2002.tb00260.x.
[12] K. A. Schwetz and G. Vogt, "Process for the Production of Dense Sintered Shaped Articles of Polycrystalline Boron Carbide by Pressureless Sintering: United States Patent.".
[13] S.L. Dole, S. Prochazka, R.H. Doremus, Microstructural coarsening during sintering of boron carbide, J. Am. Ceram. Soc. 72 (6) (1989) 958–966, https://doi.org/10.1111/j.1151-2916.1989.tb06252.x.
[14] A. Gibson, Flash Sintering of SiC Ceramics with Boron and Carbon Sintering Aids, DPhil Thesis, University of Oxford, Oxford, 2023.
[15] V.M. Candelario, R. Moreno, R.I. Todd, A.L. Ortiz, Liquid-phase assisted flash sintering of SiC from powder mixtures prepared by aqueous colloidal processing, J. Eur. Ceram. Soc. 37 (2) (Feb. 2017) 485–498, https://doi.org/10.1016/j.jeurceramsoc.2016.08.024.
[16] T. Saunders, S. Grasso, M.J. Reece, Plasma formation during electric discharge (50 V) through conductive powder compacts, J. Eur. Ceram. Soc. 35 (3) (Mar. 2015) 871–877, https://doi.org/10.1016/j.jeurceramsoc.2014.09.022.
[17] Y. Li, et al., Flash sintering of high-purity alumina at room temperature, Journal of Advanced Ceramics 12 (12) (Dec. 2023) 2382–2388, https://doi.org/10.26599/JAC.2023.9220816.
[18] Y. Li, C. Xu, R. Huang, X. Zhao, X. Wang, Z. Jia, Mechanism analysis of arc-induced flash sintering of 3YSZ at room temperature, J. Eur. Ceram. Soc. 43 (15) (Dec. 2023) 7033–7040, https://doi.org/10.1016/j.jeurceramsoc.2023.07.019.
[19] Y. Zhu, et al., Gas-discharge induced flash sintering of YSZ ceramics at room temperature, Journal of Advanced Ceramics 11 (4) (Apr. 2022) 603–614, https://doi.org/10.1007/s40145-021-0561-3.
[20] A. Wu, et al., High-performance ZnO varistor ceramics prepared by arc-induced flash sintering with low energy consumption at room temperature, High Volt. 7 (2) (Apr. 2022) 222–232, https://doi.org/10.1049/hve2.12161.
[21] C. Bechteler, A. Gibson, S. Falco, A. Kirkpatrick, R.I. Todd, Plasma formation during flash sintering of boron carbide - Part I: plasma characteristics, Ceram. Int. (May 2024), https://doi.org/10.1016/j.ceramint.2024.05.250.
[22] R. Raj, Joule heating during flash-sintering, J. Eur. Ceram. Soc. 32 (10) (2012) 2293–2301, https://doi.org/10.1016/j.jeurceramsoc.2012.02.030.
[23] F. Kaminga, S. Sato, Y. Okamoto, Evaluation of gap heat transfer between boron carbide pellet and cladding in control rod of FBR, J. Nucl. Sci. Technol. 29 (2) (1992) 121–130, https://doi.org/10.1080/18811248.1992.9731504.
[24] C.D. Wagner, A.V. Naumkin, A. Kraut-Vass, J.W. Allison, C.J. Powell, J.R. Jr. Rumble, NIST Standard Reference Database 20Version, 3, 2003, p. 4.
[25] R.I. Todd, E. Zapata-Solvas, R.S. Bonilla, T. Sneddon, P.R. Wilshaw, Electrical characteristics of flash sintering: thermal runaway of Joule heating, J. Eur. Ceram. Soc. 35 (6) (2015) 1865–1877, https://doi.org/10.1016/j.jeurceramsoc.2014.12.022.
[26] I.J. Hewitt, A.A. Lacey, R.I. Todd, A mathematical model for flash sintering, Math. Model Nat. Phenom. 10 (6) (2015) 77–89, https://doi.org/10.1051/mmnp/201510607.
[27] Y. Zhang, J.-I. Jung, J. Luo, Thermal runaway, flash sintering and asymmetrical microstructural development of ZnO and ZnO-Bi2O3 under direct currents, Acta Mater. 94 (2015) 87–100, https://doi.org/10.1016/j.actamat.2015.04.018.
[28] F. Thévenot, Boron carbide - a comprehensive review, J. Eur. Ceram. Soc. 6 (4) (1990) 205–225, https://doi.org/10.1016/0955-2219(90)90048-K.
[29] V. Domnich, S. Reynaud, R.A. Haber, M. Chhowalla, Boron carbide: structure, properties, and stability under stress, J. Am. Ceram. Soc. 94 (11) (2011) 3605–3628, https://doi.org/10.1111/j.1551-2916.2011.04865.x.
[30] D.R. Tallant, T.L. Aselage, A.N. Campbell, D. Emin, Boron carbide structure by Raman spectroscopy, Phys. Rev. B 40 (8) (Sep. 1989) 5649–5656, https://doi.org/10.1103/PhysRevB.40.5649.
[31] H. Werheit, H.W. Rotter, S. Shalamberidze, A. Leithe-Jasper, T. Tanaka, Gap-state related photoluminescence in boron carbide, Phys. Status Solidi 248 (5) (May 2011) 1275–1279, https://doi.org/10.1002/PSSB.201046342.
[32] H. Werheit, et al., On surface Raman scattering and luminescence radiation in boron carbide, J. Phys. Condens. Matter 22 (4) (Feb. 2010) 045401, https://doi.org/10.1088/0953-8984/22/4/045401.
[33] H. Werheit, On excitons and other gap states in boron carbide, J. Phys. Condens. Matter 18 (47) (Nov. 2006) 10655–10662, https://doi.org/10.1088/0953-8984/18/47/011.
[34] C. Bechteler, A. Kirkpatrick, R.I. Todd, Visible light emissions during flash sintering of 3YSZ are thermal radiation, Scripta Mater. 219 (2022), https://doi.org/10.1016/j.scriptamat.2022.114849.
[35] C. Bechteler, A. Kirkpatrick, R.I. Todd, "Comment on 'Flash in argon atmosphere yields electronically conducting yttria-stabilized zirconia at ambient temperature' by Jo et al, J. Am. Ceram. Soc. 106 (2023) 5133–5139, https://doi.org/10.1111/jace.19593. " *Journal of the American Ceramic Society*, Dec. 2023.
[36] M. Biesuz, P. Luchi, A. Quaranta, A. Martucci, V.M. Sglavo, Photoemission during flash sintering: an interpretation based on thermal radiation, J. Eur. Ceram. Soc. 37 (9) (Aug. 2017) 3125–3130, https://doi.org/10.1016/J.JEURCERAMSOC.2017.03.050.
[37] C. Bechteler, R.I. Todd, Lattice modification of ZrO2-δ and formation of rocksalt structure ZrO and Zr(O,N) after DC electrical loading of 3YSZ, J. Eur. Ceram. Soc. (Sep. 2023), https://doi.org/10.1016/J.JEURCERAMSOC.2023.09.014.
[38] M. Biesuz, P. Luchi, A. Quaranta, V.M. Sglavo, Theoretical and phenomenological analogies between flash sintering and dielectric breakdown in α-alumina, J. Appl. Phys. 120 (14) (Oct. 2016) 145107, https://doi.org/10.1063/1.4964811.
[39] K. Takahashi, Wide Bandgap Semiconductors, Springer Berlin Heidelberg, Berlin, Heidelberg, 2007, https://doi.org/10.1007/978-3-540-47235-3.
[40] C. Persson, U. Lindefelt, Detailed band structure for 3C-, 2H-, 4H-, 6H-SiC, and Si around the fundamental band gap, Phys. Rev. B 54 (15) (Oct. 1996) 10257–10260, https://doi.org/10.1103/PhysRevB.54.10257.
[41] M. Biesuz, et al., Thermally-insulated flash sintering, Scripta Mater. 162 (Mar. 2019) 99–102, https://doi.org/10.1016/j.scriptamat.2018.10.042.
[42] S.L. Dole. Ph.D. Thesis, 1985. Troy, NY.
[43] S.L. Dole, S. Prochazka, Densification and microstructure development in boron carbide, in: W. Smothers (Ed.), Proceedings of the 9th Annual Conference on Composites and Advanced Ceramic Materials: Ceramic Engineering and Science Proceedings, Ceramic Engineering and Science Proceedings, 6, John Wiley & Sons, Inc, 1985, pp. 1151–1160, https://doi.org/10.1002/9780470320280.ch65. Issue 7/8, vol. 6, vol. 6. , Hoboken, NJ, USA.
[44] I. Wynn Jones, L.J. Miles, Production of beta- Al2O3 electrolyte, Proc. Br. Ceram. Soc. (19) (1971) 161–178.
[45] M.P. Harmer, R.J. Brook, Fast firing - microstructural benefits, Trans. J. Br. Ceram. Soc. 80 (5) (1981) 147–148.
[46] M. Harmer, E.W. Roberts, R.J. Brook, Rapid sintering of pure and doped alpha-Al2O3, Trans. J. Br. Ceram. Soc. 78 (1) (Jan. 1979) 22–25.
[47] E.L. Kemer, D.L. Johnson, Microwave plasma sintering of alumina, Am. Ceram. Soc. Bull. 64 (8) (Aug. 1985) 1132–1136.
[48] W. Ji, B. Parker, S. Falco, J.Y. Zhang, Z.Y. Fu, R.I. Todd, Ultra-fast firing: effect of heating rate on sintering of 3YSZ, with and without an electric field, J. Eur. Ceram. Soc. 37 (6) (Jun. 2017) 2547–2551, https://doi.org/10.1016/J.JEURCERAMSOC.2017.01.033.
[49] W. Ji, J. Zhang, W. Wang, Z. Fu, R.I. Todd, The microstructural origin of rapid densification in 3YSZ during ultra-fast firing with or without an electric field,

J. Eur. Ceram. Soc. 40 (15) (Dec. 2020) 5829–5836, https://doi.org/10.1016/j.jeurceramsoc.2020.07.027.
[50] K.A. Schwetz, W. Grellner, The influence of carbon on the microstructure and mechanical properties of sintered boron carbide, Journal of the Less Common Metals 82 (1981) 37–47, https://doi.org/10.1016/0022-5088(81)90195-8.
[51] L.S. Sigl, Processing and mechanical properties of boron carbide sintered with TiC, J. Eur. Ceram. Soc. 18 (11) (1998) 1521–1529, https://doi.org/10.1016/S0955-2219(98)00071-5.
[52] H. Suzuki, T. Hase, T. Maruyama, Effect of carbon on sintering of boron carbide: (Japanese), Ceram Soc Jpn 87 (8) (1979) 430–433.
[53] J.R. Roth, *Industrial Plasma Engineering: Volume 1 - Principles*, Repr, Inst. of Physics Publ, Bristol, 2000.
[54] J.R. Roth, Industrial Plasma Engineering: Volume 2 - Applications to Nonthermal Plasma Processing, first ed., CRC Press, London, 2001 [Online]. Available: https://ebookcentral.proquest.com/lib/gbv/detail.action?docID=5118531.
[55] A.K. Suri, C. Subramanian, J.K. Sonber, T.S.R.C. Murthy, Synthesis and consolidation of boron carbide: a review, Int. Mater. Rev. 55 (1) (2010) 4–40, https://doi.org/10.1179/095066009X12506721665211.
[56] J.E. Zorzi, C.A. Perottoni, J.A.H. da Jornada, Hardness and wear resistance of B4C ceramics prepared with several additives, Mater. Lett. 59 (23) (Oct. 2005) 2932–2935, https://doi.org/10.1016/j.matlet.2005.04.047.
[57] T.K. Roy, C. Subramanian, A.K. Suri, Pressureless sintering of boron carbide, Ceram. Int. 32 (3) (2006) 227–233, https://doi.org/10.1016/j.ceramint.2005.02.008.
[58] A.V. Gubarevich, G. Homma, K. Yoshida, Boron carbide with improved mechanical properties fabricated via rapid pressureless densification with electromagnetic induction assistance, Scripta Mater. 238 (Jan. 2024) 115731, https://doi.org/10.1016/j.scriptamat.2023.115731.
[59] H. Martin, B. Feng, A. Michaelis, Pressureless sintering and properties of boron carbide composite materials, Int. J. Appl. Ceram. Technol. 17 (2) (Mar. 2020) 407–412, https://doi.org/10.1111/ijac.13423.
[60] W. Zhang, S. Yamashita, H. Kita, Progress in pressureless sintering of boron carbide ceramics - a review, Adv. Appl. Ceram. 118 (4) (2019) 222–239, https://doi.org/10.1080/17436753.2019.1574285.
[61] G. Liu, S. Chen, Y. Zhao, Y. Fu, Y. Wang, The effect of transition metal carbides MeC (Me = Ti, Zr, Nb, Ta, and W) on mechanical properties of B4C ceramics fabricated via pressureless sintering, Ceram. Int. 46 (17) (2020) 27283–27291, https://doi.org/10.1016/j.ceramint.2020.07.213.
[62] Y. Zhu, F. Wang, Y. Wang, H. Cheng, D. Luo, Y. Zhao, Mechanical properties and microstructure evolution of pressureless-sintered B4C-SiC ceramic composite with CeO2 additive, Ceram. Int. 45 (12) (Aug. 2019) 15108–15115, https://doi.org/10.1016/j.ceramint.2019.04.251.
[63] B.M. Moshtaghioun, D. Gomez-Garcia, A. Dominguez-Rodriguez, Richard I. Todd, Grain size dependence of hardness and fracture toughness in pure near fully-dense boron carbide ceramics, J. Eur. Ceram. Soc. 36 (7) (Jun. 2016) 1829–1834, https://doi.org/10.1016/j.jeurceramsoc.2016.01.017.
[64] U. Anselmi-Tamburini, Z.A. Munir, Y. Kodera, T. Imai, M. Ohyanagi, Influence of synthesis temperature on the defect structure of boron carbide: experimental and modeling studies, J. Am. Ceram. Soc. 88 (6) (Jun. 2005) 1382–1387, https://doi.org/10.1111/j.1551-2916.2005.00245.x.
[65] K.H.G. Ashbee, Defects in boron carbide before and after neutron irradiation, Acta Metall. 19 (10) (Oct. 1971) 1079–1085, https://doi.org/10.1016/0001-6160(71)90040-X.
[66] T. Sano, C.L. Randow, The effect of twins on the mechanical behavior of boron carbide, Metall. Mater. Trans. 42 (3) (Mar. 2011) 570–574, https://doi.org/10.1007/s11661-010-0548-0.
[67] X. Du, et al., Hot-pressing kinetics and densification mechanisms of boron carbide, J. Am. Ceram. Soc. 98 (5) (May 2015) 1400–1406, https://doi.org/10.1111/jace.13483.
[68] B.M. Moshtaghioun, D.G. García, A.D. Rodríguez, N.P. Padture, High-temperature creep deformation of coarse-grained boron carbide ceramics, J. Eur. Ceram. Soc. 35 (5) (May 2015) 1423–1429, https://doi.org/10.1016/j.jeurceramsoc.2014.11.001.